

# Development of an Apparatus for Cooling ${}^6\text{Li}$ – ${}^{87}\text{Rb}$ Fermi–Bose Mixtures in a Light-Assisted Magnetic Trap

M. Brown-Hayes<sup>a</sup>, Q. Wei<sup>a</sup>, W.-J. Kim<sup>a</sup>, and R. Onofrio<sup>a, b, c, \*</sup>

<sup>a</sup> *Department of Physics and Astronomy, Dartmouth College, 6127 Wilder Laboratory, Hanover, NH 03755 United States*

<sup>b</sup> *Dipartimento di Fisica G. Galilei, Università di Padova, Via Marzolo 8, Padova, 35131 Italy*

<sup>c</sup> *Center for Statistical Mechanics and Complexity, INFN-CNR, Unità di Roma 1, Roma, 00185 Italy*

\*e-mail: onofrio@determouth.edu

Received November 3, 2006

**Abstract**—We describe an experimental setup designed to produce ultracold trapped gas clouds of fermionic  ${}^6\text{Li}$  and bosonic  ${}^{87}\text{Rb}$ . This combination of alkali metals has the potential to reach deeper Fermi degeneracy with respect to other mixtures since it allows for improved heat capacity matching which optimizes sympathetic cooling efficiency. Atomic beams of the two species are independently produced and then decelerated by Zeeman slower. The slowed atoms are collected into a magneto-optical trap and then transferred into a quadrupole magnetic trap. An ultracold Fermi gas with temperature in the  $10^{-3}T_F$  range should be attainable through selective confinement of the two species via a properly detuned laser beam focused in the center of the magnetic trap.

PACS numbers: 03.75.Ss, 05.30.Jp, 32.80.Pj, 67.90.+z

DOI: 10.1134/S1054660X07040330

## 1. INTRODUCTION

The study of superfluidity in ultracold gases has become a rich subfield at the border between atomic physics and condensed matter physics [1]. Precision techniques characteristic of atomic physics, controllable environments for the dynamics of cold atoms, and the availability of continuous tuning of their interactions have all provided strong impetus for this research which maps into the fundamental features of high-temperature superconductivity, still an open problem in physics after more than two decades since its discovery [2]. Superfluidity and vortices in Bose gases have been studied since 1999 [3, 4], and while degenerate Fermi gases were first produced in the same year [5], only more recently has Fermi superfluid behavior been evidenced through the generation of vortices in fermionic  ${}^6\text{Li}$  [6]. This time gap in the study of weakly interacting Fermi gases with respect to their bosonic counterparts is mainly due to difficulty in the adaptation of successful boson cooling techniques to fermionic species. In particular, the Pauli principle inhibits efficient evaporative cooling among identical fermions when they reach degeneracy. Two solutions to this basic limitation have been realized, namely, mutual evaporative cooling of fermions in two different states, and sympathetic cooling of the fermions with a Bose species having a large heat capacity. In spite of these ingenious techniques, the smallest Fermi degeneracy available to date is in the  $T/T_F \approx 5 \times 10^{-2}$  range [7, 8]. This limitation has not precluded the study of interesting temperature-independent features of Fermi gases, such as quantum phase transitions related to unbalanced spin populations [9–12] and the decoherence of a Bose gas in optical lattices

filled with Fermi impurities [13, 14]. However, the study of phase transitions in which temperature is the key parameter is still unexplored territory. This will require, as discussed in [15, 16], the achievement of temperatures corresponding to  $T/T_F$  in the  $10^{-3}$  range or even lower. Unconventional pairing mechanisms, which can be unstable at higher temperatures, could then be observed, and the phase diagram of Fermi atoms in the degenerate regime could be established in a wider range of parameter space. Here, we describe the strategy and the status of an ongoing effort at Dartmouth College to reach lower degeneracy factors using fermionic  ${}^6\text{Li}$  sympathetically cooled with  ${}^{87}\text{Rb}$ . The paper is organized as follows: in Section 2, we briefly recall the current limitations in reaching a deeper Fermi degenerate regime and the motivations for choosing the  ${}^6\text{Li}$ – ${}^{87}\text{Rb}$  mixture. Section 3 is devoted to a detailed description of the apparatus, including the oven and the Zeeman slower for each species, the vacuum chamber, the pumping system, the lasers, and the frequency synthesis scheme. In Section 4, we describe plans for a light-assisted magnetic trap which should allow us to reach the targeted Fermi degeneracy. In the conclusions, we place our research project in the broader context of the study of ultracold Fermi gases and briefly discuss future physics goals.

## 2. LIMITATIONS TO REACH DEEPER FERMI DEGENERACY

As mentioned earlier, all experiments studying ultracold Fermi gases have, so far, been unable to reach a temperature lower than about 5% of the Fermi tem-

perature,  $T/T_F = 5 \times 10^{-2}$ . It is important to understand the limiting factors. In the case of dual evaporative cooling, one performs a selective removal of the most energetic fermions in both the hyperfine states. Provided that the initial number of atoms in each state is roughly the same, efficient dual evaporative cooling can be performed since the heat capacities are comparable during the entire process. This has the drawback that the number of available atoms progressively decreases over time, and, correspondingly, so does the Fermi temperature (proportional to  $N_F^{1/3}$ ). As a result, the relative gain in terms of a lower  $T/T_F$  ratio will be marginal, and the smaller clouds obtained at the end of the evaporative cooling can be detrimental to detailed experimental investigations requiring a large number of atoms. In the case of Bose-driven sympathetic cooling, the number of fermions is instead kept constant (apart from unavoidable losses due to background pressure and two- and three-body collisions), and the cooling efficiency now depends on the comparison between the fermion heat capacity and that of the Bose coolant. Unfortunately, in the degenerate regime the heat capacity of a Bose gas decreases faster than that of the Fermi gas as the cooling proceeds towards the lowest temperatures. Even in a simplified thermodynamic approach, with noninteracting Fermi and Bose gases, the crossover between the heat capacities (assuming equal trapping strengths and similar number of atoms for the two species) occurs around 5–30% of the Fermi temperature [17, 18], in line with what has been experimentally observed so far. One solution to this issue consists of intentionally unbalancing the degeneracies, keeping the Bose gas less degenerate (i.e., more classical) with respect to the Fermi gas. More classicality can be achieved by using a more massive species and/or by weakening the harmonic confinement of the Bose species relative to that of its Fermi counterpart [19]. Such species-selective trapping may be achieved via a light beam that is blue-detuned only relative to the Bose species. To quantitatively assess the cooling strategy, we have examined the choice of species and determined optimal trapping parameters [20]. Our comparison was narrowed to fermionic  ${}^6\text{Li}$  cooled through bosonic  ${}^{23}\text{Na}$ ,  ${}^{87}\text{Rb}$ , and  ${}^{133}\text{Cs}$ , but the results can be generalized to other combinations of species such as those involving  ${}^{40}\text{K}$  as the fermionic counterpart and also species recently brought to degeneracy,  ${}^3\text{He}$  [21] and  ${}^{173}\text{Yb}$  [22]. A significant improvement in the cooling efficiency can be achieved for large trapping frequency ratios, with gravitational sagging providing an upper bound, such that there will be an optimal value of the trapping frequency ratio in the range of  $\omega_F/\omega_B \approx 10$ . It turns out that the  ${}^6\text{Li}$ - ${}^{87}\text{Rb}$  mixture outperforms the other two possibilities,  ${}^6\text{Li}$ - ${}^{23}\text{Na}$  and  ${}^6\text{Li}$ - ${}^{133}\text{Cs}$ , as it has a large mass ratio with respect to the former, and at the same time mitigates the gravitational sagging with respect to the latter. Additionally, the cooling efficiency benefits from the larger

spatial overlap between the two species and from the mitigation of Fermi hole losses [23].

### 3. AN APPARATUS FOR TRAPPING AND COOLING ${}^6\text{Li}$ AND ${}^{87}\text{Rb}$

Our system is constructed using individual effusive ovens and Zeeman slower beamlines for  ${}^6\text{Li}$  and  ${}^{87}\text{Rb}$ , which are then joined in a common trapping chamber. This configuration has several advantages, including a simpler, single-species oven design and a greater ability to optimize for each species, as well as allowing for independent operation of the beamlines. Single-species ovens are also more practical due to the large difference in operating temperatures for lithium (450°C) and rubidium (100°C), as compared to double-species ovens for lithium and sodium operating at 390 and 360°C, respectively [27]. In the only other experiment using  ${}^6\text{Li}$  and  ${}^{87}\text{Rb}$  carried out at Tübingen, a Zeeman slower for lithium was used in conjunction with a rubidium getter to achieve Fermi and Bose degeneracy [24]. With respect to the experiment in Tübingen, our approach should allow for a larger ensemble of rubidium atoms and, therefore, a greater cooling capability. Figure 1 illustrates the main part of the apparatus. For each species, an effusive atomic beam is generated in the oven and Zeeman slowed before reaching the common science chamber, where the atoms are trapped in a magneto-optical trap (MOT). The main vacuum chamber is shown in Fig. 2 consisting of orthogonal pairs of 2.75-in. CF flanges for the lithium and rubidium beamlines and Zeeman viewports, as well as six flanges for the MOT viewports. All viewports on the main chamber have a broadband antireflective coating centered around 700 nm. The main chamber also has four 1.33-in. viewport flanges for optical diagnostics.

#### 3.1. Effusive Atomic Ovens

Atoms escape through a 3 mm hole made in a blank copper gasket part of the heated oven, forming an effusive atomic beam after passing through collimation elements. Rubidium has a higher vapor pressure ( $\sim 3 \times 10^{-7}$  Torr at 100°C) as compared to lithium or sodium, which is incompatible with the UHV requirement for the science chamber, and, as such, a careful oven design is needed. A double cold plate (item 4 in Fig. 3) cooled to  $\approx 0^\circ\text{C}$  through a liquid nitrogen ( $\text{LN}_2$ ) cold finger to reduce atomic vapor in the oven chamber, both improving the operating vacuum and reducing the degree of potential alkali poisoning of the ion pump during operation. After baking out the chamber, we have achieved pressures lower than  $7 \times 10^{-9}$  Torr. Even with the oven running at the extreme temperature of 180°C (compared to nominal operating temperatures of 110–150°C) the cold plate/ion pump combination maintained a pressure of  $8 \times 10^{-7}$  Torr. The estimated differential pumping ratio is  $\approx 10^2$ , with the Zeeman slower

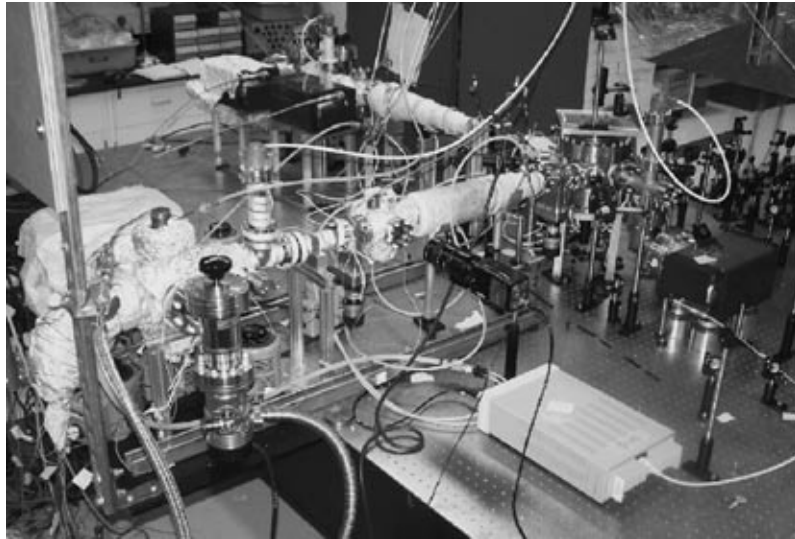


**Fig. 1.** Picture of the vacuum system, with the two orthogonal beamlines for  $^{87}\text{Rb}$  (top left) and  $^6\text{Li}$  (center). The two slower converge into the vacuum chamber for simultaneous trapping of the mixture. The apparatus can be operated in single-species mode by switching off the gate valves, one of which is visible on the lithium line just before the main chamber.

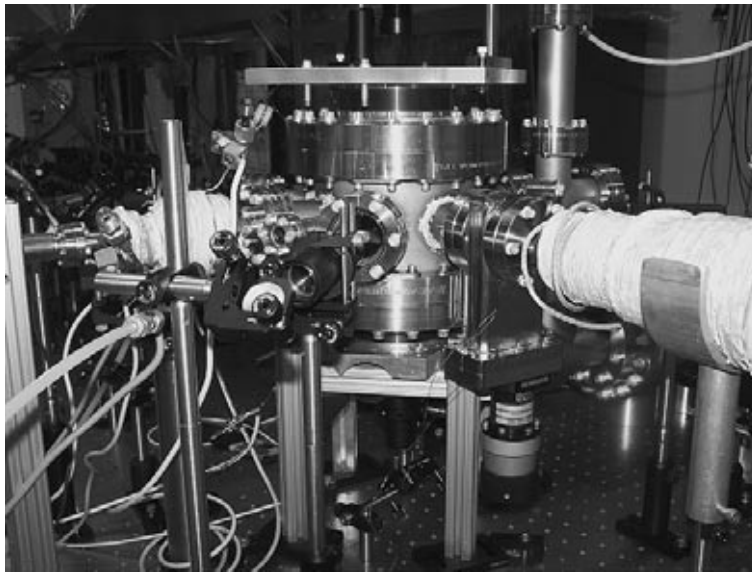


**Fig. 2.** Close up picture of the MOT vacuum chamber. On the left is the small coil for the increasing field part of the Rb Zeeman slower, while, on the right side, the final part of the decreasing field Zeeman slower for Li is visible. The vacuum chamber is sandwiched above and below by the MOT coils, together with aluminum platforms used to mount optics and to provide large surfaces for air cooling of the MOT coils.

tube itself providing another factor of 4. We have measured a total pressure ratio of  $10^3$  between the oven and the MOT chamber and believe that the presence of minor leaks in the MOT chamber is the current limiting factor. The current vacuum in the main chamber is still sufficient for efficient operation of the MOT.

Rubidium is highly reactive and, if exposed to air in the standard laboratory environment, can present a serious safety hazard. As such, an improvised tent is sealed around the oven region and kept at positive Ar pressure

throughout the loading procedure, which consists of breaking a sealed glass 5-g rubidium ampule, placing the rubidium in the oven cup, then sealing the oven elbow flange, all within the Ar tent. In other experiments [25, 26], the ampule is inserted and then broken under vacuum, which has the advantage of a cleaner Rb sample, but is mechanically more complicated and has a higher leak risk due to the use of a bellow. In either case, it is vital that the exterior of the glass ampule is cleaned thoroughly to prevent contamination, since

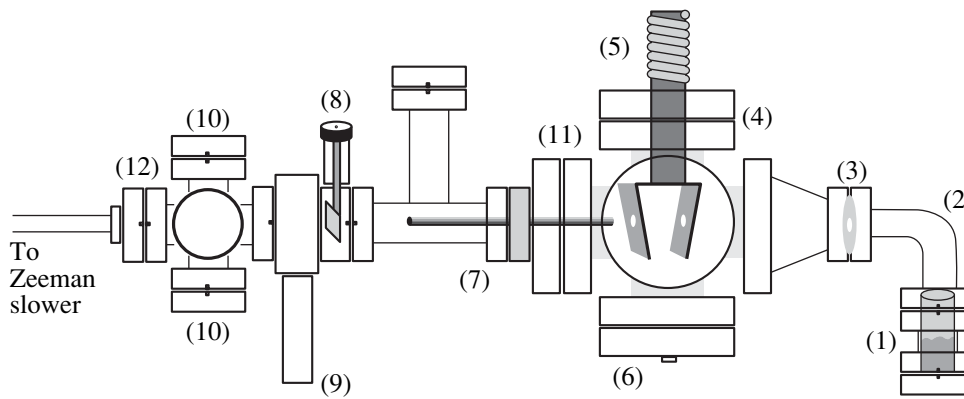


**Fig. 3.** Schematic of rubidium oven and beam preparation chamber. The metal is placed in a sample cup (1) which is inserted into the oven nipple (2). A blank copper gasket (3) with a 3 mm center hole provides the first element of collimation. Further collimation is provided by a double cold plate (4) attached to the LN<sub>2</sub>-cooled copper cold finger (5). Argon/dry nitrogen is pumped in through (6) during atom sample changes. A differential pumping tube (7) allows for the required pressure gradient between oven and science chamber, with beam shutter (8) and gate valve (9) providing beam and vacuum monitoring. Preslower diagnostic viewports (10) also help with rough alignment, and ion pumps are indicated as behind the large (11) and diagnostic (12) six-way crosses.

even a small amount of rubidium oxide will seal the sample and significantly reduce the atomic flux. We have also succeeded in melting the rubidium (melting point 39.31°C) while still inside the glass ampule and pouring it into the sample cup, which is then inserted into the elbow, again with the whole procedure conducted inside the positive-pressure Ar tent.

The lithium oven is constructed in the same manner as for rubidium, though with a few additional considerations. As already noted, lithium has a lower vapor pressure with respect to rubidium at a given temperature, and this requires a much higher operating temperature (450°C) to obtain a beam of comparable flux. At these temperatures, the copper gaskets can bond with the flange knife edges, while lithium can alloy with nickel gaskets and potentially diffuse through them [27]. Careful selection of nickel gaskets and the use of 316 stainless steel flanges solve the problem. In our case, we do not require high atomic flux— $10^6$ – $10^7$  trapped atoms in the MOT should be sufficient for our initial physics goals—and, therefore, the oven may be operated at lower temperatures.

### 3.2. Zeeman Slowers

We use Zeeman slower for both atomic beams, compensating for the Doppler shift of the progressively slowed atoms with a Zeeman shift due to an external magnetic field, such that the atoms are always kept in resonance on the cyclic transition. Zeeman slower are relatively simple to construct, usually more efficient than other methods such as chirped [28] or broadband [29] slowing, and allow for the continuous slowing of  $10^9$  atoms/s from (300–1200 m/s) to the MOT capture velocity (10–60 m/s). The maximum deceleration of the atoms in the Zeeman slower with infinite laser power is  $a_{\max} = \hbar k \Gamma / 2m$  with natural linewidth  $\Gamma$

(6.06 and 5.87 MHz for the  $^{87}\text{Rb}$  and  $^6\text{Li}$  D2 transitions, respectively) and atomic mass  $m$ ;  $a_{\max} = 1.085 \times 10^5 \text{ m/s}^2$  for Rb and  $1.82 \times 10^6 \text{ m/s}^2$  for lithium. A decreasing field slower is used for lithium, while for rubidium we use a spin-flip slower. The latter combines the advantages of a decreasing field (smaller laser detuning) with increasing field (rapid decay of fringing fields) slower designs, at the cost of a slightly higher complexity in construction.

The optimal length for the rubidium slower was evaluated to be  $\approx 70$  cm; a more cautious design called for 80 cm, allowing for finite laser power and imperfections in the slower solenoid. Atoms are slowed from  $\approx 340$  m/s to roughly 50 m/s. The main portion of the slower is 57 cm long, consisting of up to ten layers of square hollow-core copper wire, wound on a 1-in. OD brass tube, building up the desired magnetic field profile. The second smaller 13-cm section consists of a two-layer bias solenoid from which the desired profile is subtracted with a second, increasing field solenoid. Two small countercoils are used to zero the magnetic field in the gap between the two sections. The magnetic field profile is shown in Fig. 4 (measured off-line, before installation) along with the ideal target profile. To allow for both ease of installation and oven-slower-chamber alignment corrections, a 10-cm long 1.33 in. CF baffle is used between the two slower sections.

Because we use a decreasing magnetic field slower, the slower light beam is  $\sigma^+$ -polarized, utilizing the cycling transition  $F = 2, m_F = 2 \rightarrow F' = 3, m_F = 3$  (see Section 3.3 below for details of the optical pumping scheme). The longitudinal magnetic field inside the slower provides a well-defined quantization axis, and the combination of slower beam polarization and Zeeman splitting serves to minimize losses due to atoms being optically pumped out of the cycling transition. Another possible concern is transverse heating [30].

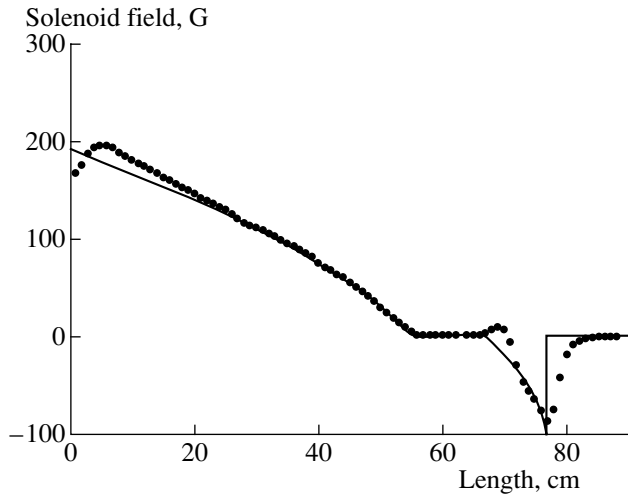


**Fig. 4.** Magnetic field profile of the rubidium spin-flip Zeeman slower, showing theoretical (solid curve) and measured (dots) profiles. The theoretical magnetic field versus the distance  $x$  along the slower, measured from its beginning, is given by  $B(x) = B_0 \sqrt{1 - 2ax/v_i^2}$ , with an offset for the gap between the two spin-flip sections, for an initial velocity  $v_i = 340$  m/s,  $B_0 = 310$  G, and a laser power of  $4I_0$  which yields a deceleration  $a = 0.8a_{\max}$ .

For the case of atoms slowed by  $v_i - v_f \approx 330$  m/s over 1.1 m, and  $v_f = 15$  m/s, the relative rms velocity is  $\Delta v_{x,y}/v_f = 5\%$ , a potentially significant loss of collimation, which can be mitigated through the implementation of transverse cooling beams sent through the six-way cross.

The much lower mass of lithium, combined with the higher operating temperature of the oven, results in a much higher initial velocity of  $v_i \sim 1000$  m/s. This requires a much stronger magnetic field (920 G) as compared to rubidium (310 G), suggesting the use of a decreasing-field slower to minimize fringing magnetic fields at the end of the deceleration stage. Our slower solenoid is constructed similarly to the main section of the rubidium slower, with 0.125 in. square, hollow copper wire wound around a 1.5-in. brass mounting tube. The slower is 36 cm long, starting with ten layers decreasing down to two, with a small countercoil at the end to limit fringing magnetic field effects. The comparison between the desired profile with the measured profile is shown in Fig. 5. The lithium slower and main and bias sections of the rubidium slower operate at currents of 35, 11, and 30 A, respectively, with the countercoils for both slowers running in the 1–5 A range. These currents are provided by 600 W–1 kW Agilent and Kepco power supplies, which require water-cooling of the coils.

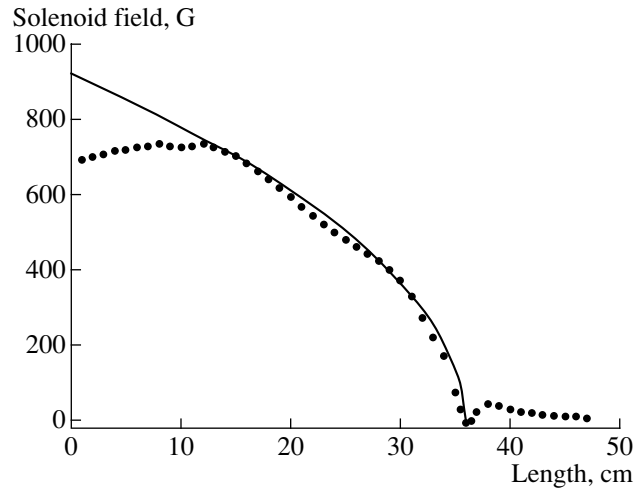


**Fig. 5.** Magnetic field profile of the lithium Zeeman slower, showing theoretical (solid line) and measured profiles (dots). The theoretical profile was conservatively calculated for atoms with initial velocity of 724 m/s, requiring a laser power of  $1.5I_0$ ,  $a = 0.6a_{\max}$ . The difference between the targeted profile and the measured one in the first 10 cm may be minimized by wrapping three extra layers of coils, which will increase the maximum capture velocity of the Zeeman slower to 887 m/s.

### 3.3. Lasers and Optics

For laser cooling of both species, we use high-power diode lasers, 350 mW at a wavelength of 780 nm for  $^{87}\text{Rb}$  and 400 mW at 671 nm for  $^6\text{Li}$  (see Fig. 6 for an overview). For each laser, the auxiliary beam (with power on the order of a few milliwatts) is used for saturation absorption spectroscopy to achieve frequency locking, while the main beam supplies the Zeeman, MOT, probe, and repumping lines. For  $^{87}\text{Rb}$ , a commercial vapor cell at room temperature is used, while for  $^6\text{Li}$ , we built a vapor cell with an operating temperature  $\sim 400^\circ\text{C}$  [31]. All the necessary frequency detunings are realized by sending the main beams through various acousto-optic modulators (AOMs), and, in the case of rubidium, also through an electro-optic modulator (EOM), with single-pass and double-pass AOM efficiencies in the 65–75 and 30–40% ranges, respectively, and repumping EOM efficiency around 3%. Once all the beams are properly detuned and polarized, they are delivered to the apparatus. Dichroic mirrors are used to combine the two sets of six beams necessary for simultaneous magneto-optical trapping of  $^6\text{Li}$  and  $^{87}\text{Rb}$ .

For  $^{87}\text{Rb}$ , a Toptica DLX110 tunable high power diode laser is locked to the crossover resonance between the  $F = 2 \rightarrow F' = 3$  and  $F = 2 \rightarrow F' = 2$  transitions at 780 nm. The laser setup for  $^6\text{Li}$  is similar to that for  $^{87}\text{Rb}$ , with a Toptica TA100 amplified tunable diode laser, which is locked to the crossover resonance between  $^6\text{Li}$   $F = 3/2 \rightarrow F' = 5/2$  and  $F = 1/2 \rightarrow F' = 5/2$  transitions at 671 nm. Figure 7 shows the frequency synthesis scheme for all required beams for both spe-

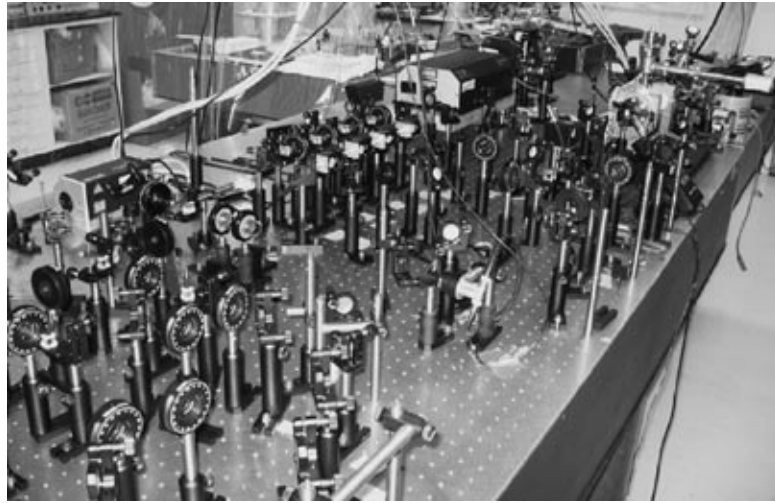


**Fig. 6.** Optical table with 671 and 780 nm laser systems, Rb and Li vapor cells for saturated absorption frequency locking, and optical elements for frequency synthesis. On the left is the 780 nm laser and related Rb vapor cell, while in the top center is the 671 nm laser, with the related Li vapor cell on its right.

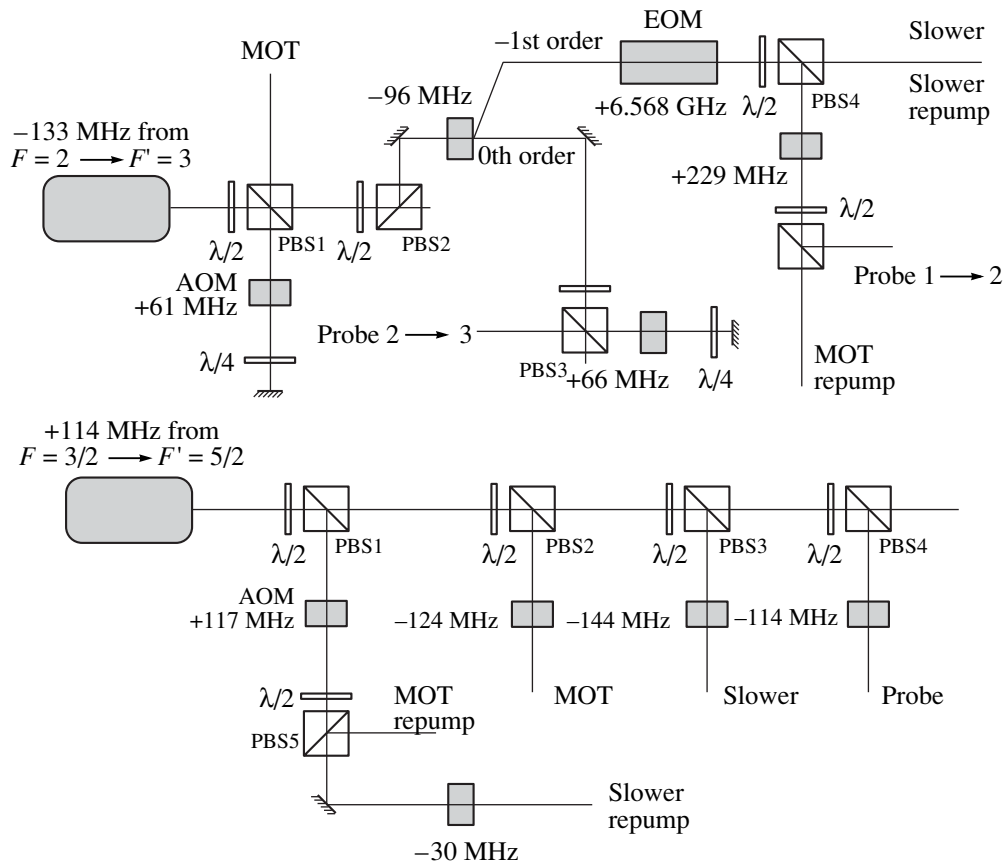


**Fig. 7.** Frequency synthesis schemes. For both species, we use 20 mW for the slower beam and 10 mW for each MOT beam, and in order to keep the transitions closed, repumping beams for the MOT and slower with 5–10% power for Rb, and 30% for Li power are also generated. For  $^{87}\text{Rb}$  (above), with AOMs and EOM providing the required detunings, the MOT and slower beams are detuned by  $-11$  and  $-229$  MHz from the  $F = 2 \rightarrow F' = 3$  transition, respectively. MOT and slower repumping beams are in resonance with and detuned by  $-229$  MHz from the  $F = 1 \rightarrow F' = 2$  transition. For  $^6\text{Li}$  (below), the MOT and slower beams are detuned by  $-10$  and  $-30$  MHz from the  $F = 3/2 \rightarrow F' = 5/2$  transition; repumping beams for the MOT and slower are in resonance with and detuned by  $-30$  MHz from the  $F = 1/2 \rightarrow F' = 3/2$  transition. Probe beams are also generated which are in resonance with each of the selected transitions.

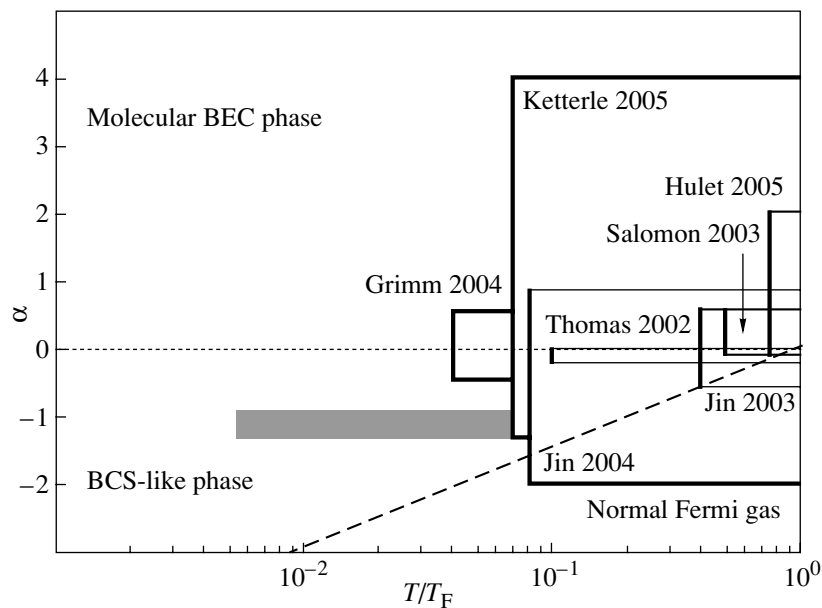


**Fig. 8.** Current status of Fermi degeneracy achieved by various groups and indication of our target domain (shaded area). The coupling strength parameter  $\alpha = 1/k_F a$ , with  $k_F$  the Fermi wave number and  $a$  the scattering length, is plotted versus the degeneracy parameter  $T/T_F$ . The dotted horizontal line at  $\alpha = 0$  separates the parameter space into the two regions of BEC molecular regime ( $\alpha > 0$ ) and BCS regime ( $\alpha < 0$ ). The dashed line, based on Eq. (3) in [33], provides further demarcation between the BCS superfluid phase (based on a critical temperature arising from s-wave pairing in the different internal states) and the normal Fermi gas phase. Our targeted region extends into  $T/T_F = 5 \times 10^{-3}$ , well within the Fermi degeneracy on the BCS side. The spread along the  $\alpha$  direction should be obtained, rather than by changing  $a$  with Feshbach resonances, by modifying  $k_F$  via different trapping strengths, varying the intensity of the deconfining laser beam. Areas labeled Grimm 2004, Ketterle 2005, Jin 2004, Thomas 2002, Jin 2003, Salomon 2003, and Hulet 2005 are from [8], [6], [34], [35, 36], [37], [38], and [39], respectively. A degeneracy factor of  $T/T_F = 5 \times 10^{-2}$  was reported in [7] without Feshbach modulation of the scattering length.

cies, and the caption includes details of beam power budget and detunings.

#### 4. DESIGN OF MAGNETO-OPTICAL AND LIGHT-ASSISTED MAGNETIC TRAPS

The Zeeman slowed  ${}^6\text{Li}$  and  ${}^{87}\text{Rb}$  atoms are captured, mixed, and precooled in the MOT. A pair of coils in anti-Helmholtz configuration produces an axial magnetic field gradient of 8 G/cm. The six-beam configuration is beneficial for achieving sub-Doppler optical molasses. After precooling and hyperfine state preparation, we will transfer the atoms to a magnetic trap using  ${}^6\text{Li}$  in the  $F = 3/2$ ,  $m_F = 3/2$  state, and either  $F = 2$ ,  $m_F = 2$  or  $F = 1$ ,  $m_F = -1$  for  ${}^{87}\text{Rb}$ , all of which are weak field seeking states. The stretched states (as used in [24]) have the advantage of minimizing spin exchange losses, while the  ${}^6\text{Li}$  ( $3/2$ ,  $3/2$ )– ${}^{87}\text{Rb}$ ( $1$ ,  $-1$ ) combination yields the maximum natural trapping frequency ratio, more than twice that of the  ${}^6\text{Li}$  ( $3/2$ ,  $3/2$ )– ${}^{23}\text{Na}$ ( $2$ ,  $2$ ) combination that has yielded a  $T/T_F = 5 \times 10^{-2}$  [7]. Our trapping scheme is inspired by the design of an optically plugged quadrupole trap (OPT) [32], but is designed for a lower power deconfining laser beam. The coils form a quadrupole magnetic field which traps low-field seeking particles, but suffers from Majorana

loss due to the magnetic field zero at the center. However, in the presence of a blue-detuned laser beam, the atoms are repelled from the center of the trap and so spin-flip related losses are reduced. The trapped rubidium will be then evaporatively cooled, in turn sympathetically cooling the fermionic lithium. As discussed above, it is advantageous to prevent the rubidium from entering a deeply Bose condensed phase, as the gas has a much higher heat capacity in the classical regime and around the Bose–Einstein phase transition.

In the OPT we are currently building, each coil has six layers of ten windings of 0.125 in. square copper tubing. The inner diameter of the coils is 3 in., and the spacing between the two coils is 2 in. This pair of coils will be used to generate the magnetic gradient field for both MOT and OPT by quickly switching the current from 10 to 200 A, which results in field gradients of 20 and 400 G/cm, respectively. A 690 nm laser provides a 35 mW beam which propagates along the axis of the coils and is focused into the center of the quadrupole trap with a waist of 40  $\mu\text{m}$ . Use of a laser beam with a wavelength in between the atomic transitions for the two species (red-detuned for  ${}^6\text{Li}$  and blue-detuned  ${}^{87}\text{Rb}$ ) will result in stronger confinement of the fermionic species, at the price of increased localization of the lithium atoms near the trap center, where Majorana

spin-flip losses become significant. However, in the degenerate regime, the Fermi gas will experience an effective Pauli repulsion and, therefore, a relatively smaller number of atoms around the trap center will be lost through Majorana spin-flips.

## 5. CONCLUSIONS

The minimum reachable Fermi degeneracy in experiments using sympathetic cooling techniques is limited by the heat capacity matching of the two species. We have described an apparatus under development to explore these concepts and aimed at reaching deeper Fermi degeneracy. The achievement of lower  $T/T_F$  is desirable for the further exploration of the BEC–BCS crossover regime. Specifically, we aim to broaden the experimental parameter space to study Fermi pairing into various superfluid phases. The parameter space of  $\alpha = 1/k_F a$  versus  $T/T_F$  achieved in various ongoing experiments is shown in Fig. 8, also including the region we propose to study. The latter is complementary to the former, in the sense that we do not intend to explore a large region of the coupling parameter  $\alpha$ , at least as far as a magnetic trap is used. We should reach  $T/T_F$  ratios an order of magnitude lower than those currently achieved. New phenomena, including a nontrivial phase for superfluidity only present at finite temperature [16, 40], are expected in the  $T/T_F$  regime which could be accessible with our technique. The use of a bichromatic optical trap configuration as discussed in [19] could extend the study to a broader range through Feshbach resonances.

As a concrete example of a research direction, we can investigate the role played by the effective mass of fermions for superfluid pairing in optical lattices. Mismatched pairing has been suggested to occur as a result of unequal cloud densities or masses, for example, a mixture of  ${}^6\text{Li}$  and  ${}^{40}\text{K}$  [41]. This mass difference could also be realized by preparing the fermions in two separate hyperfine states which have significantly different electric dipole polarizabilities. In the presence of an optical lattice, this would correspond to the two states having different effective masses. We have examined the case of two lithium hyperfine states ( $2S_{1/2}^2$  and  $2P_{1/2}^2$ ) and an effective mass ratio dependent on the two electric polarizabilities. It appears that state-selective magnetic trapping is possible with  ${}^6\text{Li}$  hyperfine states and could allow for the comparison between various exotic states of superfluids, including LOFF states [42] and their combinations [43].

More generally, superfluid Fermi–Bose mixtures may be used as an analog computer to solve equations mimicking the equations of states for quantum chromodynamics in regimes where perturbative techniques or lattice computations have not yet succeeded. The first theoretical steps in this very promising and interdisciplinary direction can be found in [44–47].

## ACKNOWLEDGMENTS

We are grateful to Richard L. Johnson for skillful technical support and high quality machining, and to David Collins for electronics design and support. M.B.H., Q.W., and W.J.K. acknowledge support from the Dartmouth College Graduate Fellowship. M.B.H. has also been supported by the NSF–GAANN and Gordon Hull Fellowship programs. R.O. acknowledges support from Dartmouth College and from MIUR, Italy, under PRIN 2004028108\_001.

## REFERENCES

1. A. L. Fetter and A. A. Svidzinsky, *J. Phys. Condens. Matter* **13**, R135 (2001); A. J. Leggett, *Rev. Mod. Phys.* **73**, 307 (2001); C. J. Pethick and H. Smith, *Bose–Einstein Condensation in Dilute Gases* (Cambridge Univ. Press, Cambridge, 2002); L. P. Pitaevskii and S. Stringari, *Bose–Einstein Condensation* (Oxford Sci. Publ., Oxford, 2003).
2. Q. Chen, J. Stajic, S. Tan, and K. Levin, *Phys. Rep.* **412**, 1 (2005).
3. M. R. Matthews, et al., *Phys. Rev. Lett.* **83**, 2498 (1999).
4. C. Raman, et al., *Phys. Rev. Lett.* **83**, 2502 (1999).
5. B. De Marco and D. S. Jin, *Science* **291**, 2570 (1999).
6. M. W. Zwierlein et al., *Science* **435**, 1047 (2005).
7. Z. Hadzibabic, S. Gupta, C. A. Stan, et al., *Phys. Rev. Lett.* **91**, 160401 (2003).
8. M. Bartenstein et al., *Phys. Rev. Lett.* **92**, 120401 (2004).
9. M. Zwierlein, A. Schirotzek, C. H. Schunck, and W. Ketterle, *Science* **311**, 492 (2006).
10. G. B. Partridge, W. Li, R. L. Kamar, et al., *Science* **311**, 503 (2006).
11. M. Zwierlein, A. Schirotzek, C. H. Schunck, and W. Ketterle, *Nature* **442**, 54 (2006).
12. Y. Shin et al., *Phys. Rev. Lett.* **97**, 030401 (2006).
13. K. Günther et al., *Phys. Rev. Lett.* **96**, 180402 (2006).
14. S. Ospelkaus et al., *Phys. Rev. Lett.* **96**, 180403 (2006).
15. Q. Chen et al., *Phys. Rev. A* **73**, 041601(R) (2006).
16. C.-C. Chien et al., *Phys. Rev. Lett.* **97**, 090402 (2006).
17. C. Presilla and R. Onofrio, *Phys. Rev. Lett.* **90**, 030404 (2003).
18. R. Onofrio and C. Presilla, *J. Stat. Phys.* **115**, 57 (2004).
19. R. Onofrio and C. Presilla, *Phys. Rev. Lett.* **89**, 100401 (2002).
20. M. Brown-Hayes and R. Onofrio, *Phys. Rev. A* **70**, 063614 (2004).
21. J. D. McNamara et al., *Phys. Rev. Lett.* **97**, 080404 (2006).
22. T. Fukuhara, Y. Takasu, M. Kumejima, and Y. Takahashi, *cond-mat/0607288* (2006).
23. R. Côté, R. Onofrio, and E. Timmermans, *Phys. Rev. A* **72**, 041605(R) (2005).
24. C. Silber et al., *Phys. Rev. Lett.* **95**, 170408 (2005).
25. E. Streed et al., *Rev. Sci. Instrum.* **77**, 023106 (2006).
26. P. D. D. Schwindt, PhD Thesis (Univ. of Colorado at Boulder, 1997).

27. C. A. Stan and W. Ketterle, *Rev. Sci. Instrum.* **76**, 063113 (2005).
28. W. Ertmer et al., *Phys. Rev. Lett.* **54**, 996 (1985).
29. M. Zhu et al., *Phys. Rev. Lett.* **67**, 46 (1991).
30. K. J. Günther, [www.quantumoptics.ethz.ch/slower.pdf](http://www.quantumoptics.ethz.ch/slower.pdf).
31. K. G. Libbrecht et al., *Am. J. Phys.* **63**, 729 (1995).
32. K. B. Davis et al., *Phys. Rev. Lett.* **75**, 3969 (1995); D. S. Naik, and C. Raman, *Phys. Rev. A* **71**, 033617 (2005).
33. M. Houbiers, R. Ferwerda, and H. T. C. Stoof, *Phys. Rev. A* **56**, 4864 (1997).
34. C. A. Regal, M. Greiner, and D. S. Jin, *Phys. Rev. Lett.* **92**, 040403 (2004).
35. K. M. O'Hara et al., *Science* **298**, 2179 (2002).
36. J. Kinast, A. Turlapov, and J. E. Thomas, *Phys. Rev. Lett.* **94**, 170404 (2005).
37. C. A. Regal and D. S. Jin, *Phys. Rev. Lett.* **90**, 230404 (2003).
38. T. Bourdel et al., *Phys. Rev. Lett.* **91**, 020402 (2003).
39. G. B. Partridge et al., *Phys. Rev. Lett.* **95**, 020404 (2005).
40. Q. Chen, J. Stajic, and K. Levin, *Phys. Rev. A* **95**, 260405 (2005).
41. W. V. Liu and F. Wilczek, *Phys. Rev. Lett.* **90**, 047002 (2003).
42. P. Fulde and R. A. Ferrell, *Phys. Rev. A* **135**, 550 (1964); A. I. Larkin and Yu. N. Ovchinnikov, *Sov. Phys. JETP*, **20**, 762 (1965).
43. J. Dukelsky, G. Ortiz, S. M. A. Rombouts, and K. Van Houcke, *Phys. Rev. Lett.* **96**, 180404 (2006).
44. L. He, M. Jin, and P. Zhuang, *Phys. Rev. B* **73**, 214527 (2006); *Phys. Rev. B* **73**, 220504(R) (2006).
45. A. Rapp, G. Zaránd, C. Honerkamp, and W. Hofstetter, *cond-mat/0607138* (2006).
46. L. He, M. Jin, and P. Zhuang, *Phys. Rev. A* **74**, 033604 (2006).
47. L. He, M. Jin, and P. Zhuang, *Phys. Rev. D* **74**, 056007 (2006).